IOP Publishing | International Atomic Energy Agency Nuclear Fusion

Nucl. Fusion 56 (2016) 056002 (18pp) doi:10.1088/0029-5515/56/5/056002

Core fusion power gain and alpha heating in JET, TFTR, and ITER

R.V. Budny[1], J.G. Cordey[2] and TFTR Team and JET Contributors[3,4]

[1] Princeton University, Princeton, NJ 08540, USA
[2] CCFE Fusion Association, Culham Science Center, Abingdon, UK
[3] EUROfusion Consortium, JET, Culham Science Centre, Abingdon, OX14 3DB, UK

E-mail: budny@princeton.edu

Received 1 October 2015, revised 12 February 2016
Accepted for publication 22 February 2016
Published 31 March 2016

Abstract

Profiles of the ratio of fusion power and the auxiliary heating power q_{DT} are calculated for the TFTR and JET discharges with the highest neutron emission rates, and are predicted for ITER. Core values above 1.3 for JET and 0.8 for TFTR are obtained. Values above 20 are predicted for ITER baseline plasmas.

Keywords: JET, TFTR, ITER, fusion power gain, alpha heating, integrated modeling, DT fusion

(Some figures may appear in colour only in the online journal)

1. Introduction

The research goal of magnetically confined tokamak discharges is to develop practical fusion devices for generating electrical power from deuterium-tritium (DT) fusion reactions. This requires that the energy released by the fusion reactions is substantially more than the power used to heat and control the plasma. This requirement can be translated into lower bounds on the fusion power gain (Q_{DT}) defined as the ratio of the fusion power (P_{DT}) relative to the external auxiliary input power ($P_{\rm ext}$). External heating and current drive are envisioned even for fusion reactors to control the plasmas. High values of Q_{DT} are required to achieve dominant self-heating of the plasma by the energetic alpha particles produced by DT fusion.

The goal of 'break-even' ($Q_{DT}=1$) has remained a milestone for controlled fusion research. If plasmas sustain $Q_{DT}\simeq 1$ for durations comparable to the slowing down time of the alphas then the alpha heating to $P_{\rm ext}$ ratio is predicted to be $\simeq$20%.

Since the alpha heating profile p_α is predicted to be core localized, core values of the profile of Q_{DT} denoted q_{DT} are interesting as a metric for the ratio of the alpha heating and external heating. High values of this ratio are necessary, but not sufficient for measuring p_α since other terms such as ion-electron heat exchange might be comparable.

Recently the National Ignition Facility (NIF) team has claimed to have achieved local break-even in the core of imploding capsules [1]. It is not generally known that tokamak experiments with deuterium and tritium have achieved local break-even (for brief durations). In this paper we compute q_{DT} in past experiments in TFTR and JET and predict this for an ITER simulation. Values of core q_{DT} near unity were achieved in TFTR and above unity in JET.

This paper studies the TFTR and JET discharges with highest Q_{DT}. Besides computing q_{DT}, the electron heat balance and alpha heating profile are discussed. The extreme conditions of these discharges were especially challenging for the diagnostic measurements, so ambiguities of the measurements and the analysis are discussed in detail here.

The TRANSP code [2, 3] is used to calculate these quantities for TFTR and JET plasmas, and to generate self-consistent, time-dependent integrated predictions for ITER plasmas. Predictions for an ITER baseline scenario are given.

Here the profile of q_{DT} is defined as the ratio of the volume-averaged DT fusion energy (alpha and neutron) production p_{DT} divided by the volume-averaged local auxiliary heating power $p_{\rm ext}$. This definition equals the usual global definition of Q_{DT} when evaluated at the plasma boundary. The use of volume-averaging has the advantage of smoothing statistical noise in the radial dimension such as Monte Carlo noise from

[4] See the appendix of [46].

the fast ion numerical computations. The limit at small radii near the core is well defined.

ITER is being constructed to study physics and technological issues for the development of fusion reactors. Among the goals [4] are the production of 400 MW of fusion energy P_{DT} for long durations (300–500 s). The goal for the global Q_{DT} in 'baseline' H-mode plasmas is 10. An alternative 'hybrid' scheme with lower plasma current ($\simeq$12 MA) is planned for studying long pulses with a goal of $Q_{DT} > 5.0$. The steady-state scenario aims at $Q_{\rm DT} \gtrsim 5.0$. These conditions should facilitate study of alpha heating. The maximum $P_{\rm ext}$ is planned to be 73 MW.

The new results in this paper are calculations of q_{DT} and alpha heating in the extreme and challenging JET and TFTR plasmas, and new predictions for an ITER baseline plasma for comparison. The next section describes methods used for the TRANSP simulations. Alternative methods are described and used to address uncertainties and lacks of measurements. Sections 3–5 give an overview of the JET plasma and discusses the simulation validity and results. Sections 6–8 do the same for the TFTR plasma. Section 9 gives a new prediction for an ITER baseline plasma and predicts q_{DT} and $p_{\alpha e}$. Section 10 gives a summary and further discussions.

2. Methods

TRANSP has been extensively improved since the TFTR and JET discharges were performed in the years 1994–1997. Important improvements include more accurate equilibrium solvers, incorporation of ADAS atomic process cross-sections [5] with self-consistent multi-step excited states ionization of beam neutrals, the ability to treat multiple impurity species, and parallelization of various modules.

Accurate treatment of multi-step excited state ionization is important since the beam deposition effects the beam ion particle, torque, and energy densities which impact the neutron emission rates, total and diamagnetic energy, and ripple losses.

New high resolution TRANSP analysis runs were done for the TFTR and JET discharges to increase the accuracy of, and confidence in the analysis. In the analysis reported here the measured profiles were input to TRANSP without radial or time smoothing other than spline fits to the data points. Typical TRANSP analysis runs use a variety of radial and/or time smoothing of data such as plasma profiles and beam waveforms to generate relatively smooth profiles of transport to facilitate the interpretation.

The auxiliary heating includes Ohmic (OH) and neutral beam (NB) heating for all plasmas considered. The OH heating is relatively small, however $p_{\rm OH}$ profiles are included in $p_{\rm ext}$ for computing q_{DT}. Orbits and interactions of the fast beam and alpha ions are computed using the parallelized NUBEAM Monte Carlo module [2, 6]. The beam and alpha ion heating of the thermal electrons, thermal ions, and their thermalization rates are computed. The fusion reaction rates of the thermal and beam-injected deuterons and tritons are based on fits [7] to cross section data.

For the JET and ITER plasmas, ion cyclotron heating (IC) is included. Profiles of the direct IC heating of the thermal electrons and thermal and fast ions are computed by the TORIC [8] full wave solver. In previous TRANSP simulations of discharges with IC and NB, the direct IC interactions with fast ions was ignored. A recent improvement in the computation of the coupling of IC acceleration/deacceleration on fast ions in TRANSP [9] is used. For this, a Monte Carlo IC kick operator has been installed in NUBEAM. This computes the acceleration or deacceleration of orbiting fast ions as they pass through the IC resonance layers. Each kick changes the magnetic moment μ, and perpendicular and parallel velocities $v_\perp$, and $v_\parallel$. The changes of energy of the D and T beam ions and fast alpha ions can be significant. The changes in the beam ions has noticeable effects on the neutron emission rates. Profiles of the IC minority ion (trace H for JET and He^3 assumed for ITER) heating are computed by the FPPRF Fokker–Planck module [10] in TRANSP.

For ITER, electron cyclotron heating EC is also included. Profiles of the EC heating of thermal electrons are computed by the TORAY [11, 12] ray tracing code in TRANSP.

The accuracy of the simulations for q_{DT} and the alpha heating profile p_α depends on the accuracy of the plasma and heating profiles. Profiles of the densities of thermal D (n_D), T (n_T), and fast D and T beam ions are needed to compute the DT fusion rate. In TRANSP the fast and thermal ions from beam injection and fusion products are treated separately. This facilitates calculations of slowing down and of neutron emission rates since the fusion cross sections depend sensitively on the ion relative velocities. The fast ions are converted to thermal after they pitch angle scatter and slow down to energies below $1.5\times$ the local thermal ion temperature T_i. This choice for separation of ion species could skew the predicted neutron emission rates, so the sensitivity was studied in [3]. A Fokker–Planck module in TRANSP was modified to improve the treatment of thermalization. This did not have a large effect compared with previous Fokker–Planck results. The energy distributions of D and T beam ions computed by the Fokker–Planck module were compared with those from the Monte Carlo module added to the thermal distributions. The results agreed well except at low energies where the Fokker–Planck results are low. This was attributed to lower beam density in the core from the neglect of beam charge exchange processes in the Fokker–Planck treatment. The pitch angle scattering rate used is from [13].

In the TRANSP analysis the electron density profile $n_{\rm e}$ is input and the thermal and fast ion species densities n_j are calculated self-consistently assuming charge neutrality and species conservation (Gauss' theorem). Multiple impurity densities can be input or calculated from a measured or assumed $Z_{\rm eff}$ profile

$$Z_{\rm eff} \equiv \sum_j n_j Z_j^2 / n_{\rm e}. \tag{1}$$

where j indicates each ion species. For the discharges studied here there were no useful $Z_{\rm eff}$ profiles from visible bremsstrahlung emission measurements, so the $Z_{\rm eff}$ profiles are computed from measured impurity densities (C in TFTR and Be and C

in JET). The source rates for the hydrogenic thermal ions are classed in TRANSP as core (fast ion thermalization, ionization, charge-exchange, pellet injection) and wall (gas puffing, recycling). For TFTR and JET analysis the wall recycling rate is estimated from hydrogenic-alpha photon emission measurements.

Modeling of TFTR discharges with the DEGAS 3D neutrals code indicates that the rate of hydrogenic ionizations within the last closed flux surface is proportional to the chordal hydrogenic-alpha photon emission [14]. The proportionality constant has been modeled for various plasma regimes. This total ionization rate at the last closed flux surface is converted to a profile in TRANSP by the FRANTIC model. Studies of recycling in JET using EDG2D indicate a similar factor for the neutral influx/hydrogenic-alpha signal [15].

The partition of the the total hydrogenic rate to H, D, and T can be set in the TRANSP namelist. The wall recycling effects plasma parameters mainly outside the half minor radius where the fusion reaction rates are small.

Although the edge H, D, and T densities are inferred from H-alpha emission measurements, there is ambiguity calculating the separate core n_D and n_T densities. Their total is constrained by charge neutrality. Their relative transport rates are predicted to be different in turbulence theories due to their different masses. Fortunately p_{DT} is insensitive to the ratio of n_D/n_T in the core when they are approximately equal.

TRANSP has models allowing assumptions of different relative convection of the hydrogenic species. Multiple variations have been tested but, due to measurement uncertainties, the tests are inclusive. The JET and TFTR discharges considered here were empirically optimized in terms of their fueling by D and T for maximal fusion power production and presumably achieved nearly equal densities of D and T in the plasma core. The particle transport models in TRANSP used here were chosen to achieve this. They derive approximately equal n_D and n_T in the core for the assumptions used.

The DT fusion rate is dominated by a low energy He^5 spin 3/2 resonance which enhances the rates at the higher energies of the beam ions. TRANSP calculates separately the D-beam-T-thermal, T-beam-D-thermal, D-beam-T-beam, and T-beam-D-beam, along with the D-thermal-T-thermal (thermonuclear) rates.

We discuss processes that can reduce the beam ion densities and energies. One is ripple loss. A simple stochastic ripple loss model for fast ions [16] has been installed in TRANSP. A ripple loss criterion using the local magnetic field toroidal variation and safety factor at the banana tips has been fine tuned using more complete calculations with the ORBIT code for some TFTR discharges [17].

Other processes such as MHD and anomalous fast ion losses can alter the beam profiles. Simulations of certain classes of discharges with neutral beam injection simulate neutron production rates significantly higher than measured. Ad hoc anomalous diffusion of beam ions has been proposed for reducing the beam density and thus reducing the simulated stored energies and neutron emission rates. Examples of studies from TFTR are reported in [18] and for JET in [19]. The TFTR and JET discharges discussed below have simulated neutron emission rates lower than measured so addition of ad hoc anomalous beam ion diffusion would make the agreement worse.

The JET study [19] reported evidence for the need for anomalous diffusion for the tritium beam ions in reverse magnetic shear discharges, hybrid discharges, and H-mode discharges, especially with high density. The issue at high density suggests that the simulated T beam deposition might be too deep. Recently the JET neutron diagnostics have been recalibrated, and the measured neutron rates in discharges after 2007 increased by 16%, reducing the needed anomalous diffusion for agreement in TRANSP.

Accurate calculations of the beam deposition are needed for accurate calculations of the beam densities. Various effects such as multi-step ionization can have significant effects, especially at high densities. Also impurity charge-exchange can have significant effects.

Tests of the validity of the TRANSP analysis include the ability to predict accurately the diamagnetic flux and stored energies, and the measured neutron emission rates and their profiles. The volume-integrated stored energies emphasize the profiles at large minor radius where the the volume elements are larger. The diamagnetic flux indicates the accuracy of the model for the thermal and perpendicular fast ion stored energies.

Instead the total neutron emission rate weighs n_D, n_T, and T_i in the core where the volume elements are relatively small. The simulated stored energy is insensitive to the mix of tritium and deuterium when other parameters are held fixed, so agreement with the neutron rate does not correlate strongly with agreement with stored energy.

3. JET discharge with record P_{DT}

The JET discharge achieving the highest global P_{DT} is a Hot-ion H-mode (discharge 42976 during the 1997 DTE1 campaign) [20]. It started with a relatively low-density Ohmically-heated plasma. The auxiliary heating consisted of up to 11.9 MW D-NB, 10.5 MW T-NB, 0.4 MW Ohmic, and 3.2 MW IC tuned to 51 MHz to resonate with hydrogen-minority ions near the plasma axis. The plasma current, major radius, and vacuum toroidal field were $I_p = 4.0$ MA, $R_0 = 2.92$ m, $B_0 = 3.82$ T. Some parameters are summarized in table 1.

The normalized total pressure (thermal plus fast ion) β_n was 1.98 and the thermal alone was 1.6. The plasma energy increased throughout an ELM-free period lasting 0.9 s. Then a series of three giant ELMs occurred starting around 13.4 s.

Profiles of the interferometry-measured n_e are shown in figure 1(a) versus $x(\equiv$ square-root of the normalized toroidal flux). The profiles are hollow throughout the NB phase. The line-averaged electron density $\overline{n}_e$ increasing to 30% of the empirical Greenwald density limit ($n_{Gw} \equiv I_p/(\pi a^2)$ (MA m^{-2})) at the end of the beam-heated phase, then increases abruptly, peaking at 0.75.

Profiles of the electron temperature T_e measured from electron-cyclotron emission are shown in figure 1(b). TRANSP maps the data from electron-cyclotron frequency to major radius. Profiles were also measured by LIDR. These were much nosier and scarcer in time and space. Both

Table 1. Summary of global and core parameters (averaged to $x = 0.2$ for TFTR and JET, and $x = 0.4$ for ITER) before the impurity bloom in TFTR and the X-event in JET.

Tokamak	B_{tor} (tesla)	I_p (MA)	H_{98y2} (—)	β_n (—)	P_{DT} (MW)	Q_{DT} (—)	f_{Gw} (—)	Peakedness (—)	Pressure (Atm)	$p_{DT}(0)$ (MW m^{-3})	$p_\alpha(0)$ (MW m^{-3})	p_α/p_{ext} (—)	$\beta_\alpha(0)$ (—)
TFTR	5.5	2.7	0.75	1.95	11.5	0.28	0.46	2.75	7.3	2.4	0.21	0.06	0.003
JET	3.8	4.2	1.05	1.98	16.5	0.68	0.30	0.8	3.6	0.6	0.09	0.18	0.006
ITER	5.3	15.0	0.92	1.85	460	10.0	0.86	1.03	7.8	2.2	0.40	3.5	0.007

Note: $f_{Gw} \equiv \bar{n}_e/n_{Gw}$. H_{98y2} is the energy confinement normalized by the H-mode database H_{98y2} fit. The peakedness in the ratio of the core to volume-averaged electron density.

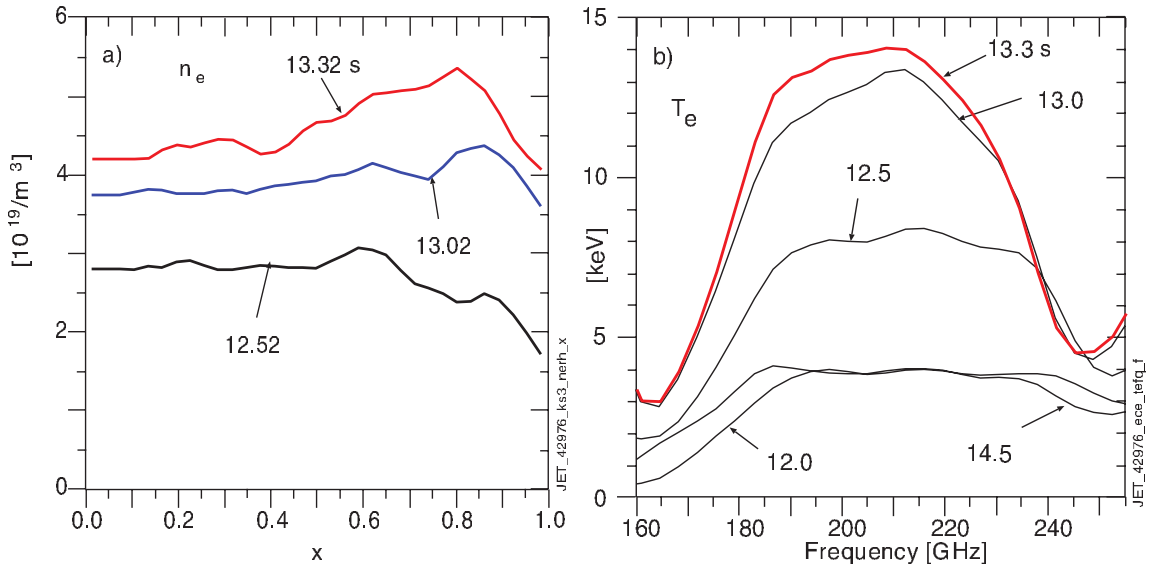

Figure 1. Profiles of the (*a*) interferometry measured n_e versus x(≡ square-root of the normalized toroidal flux) and (*b*) electron-cyclotron measured T_e versus emission frequency in JET.

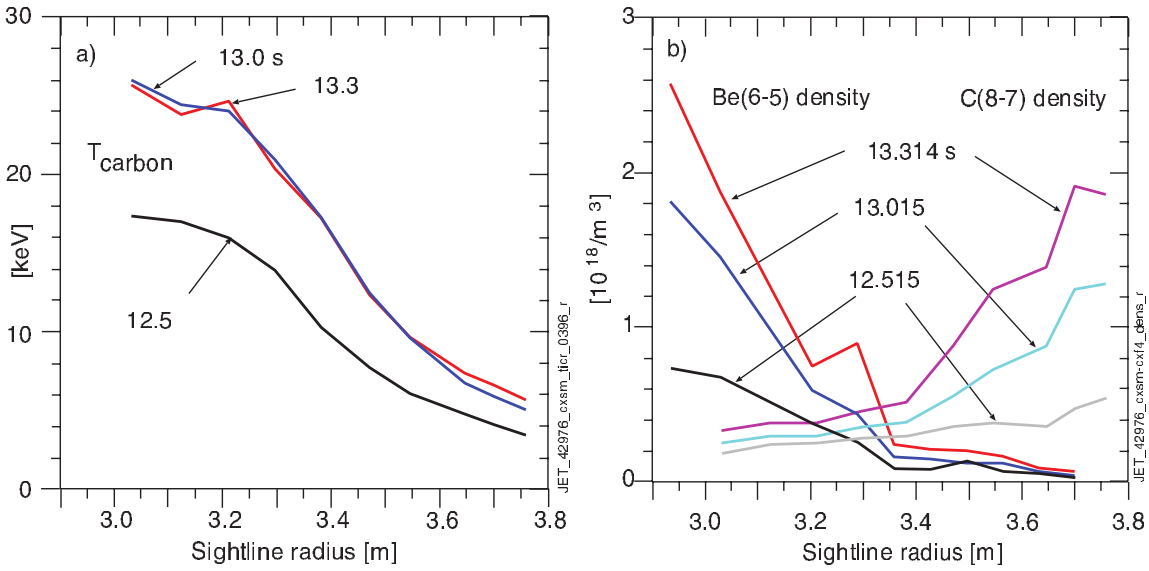

Figure 2. Profiles of the charge-exchange spectroscopy measured (*a*) T_{carbon} and (*b*) n_{Be}.

measurements were in approximate agreement for T_e except for high T_e ($\gtrsim$8 keV) where ECE gave higher values [21]. This discrepancy is not understood, but a non-Maxwellian distribution has been suspected.

Profiles of the carbon temperature, rotation, and *C*, He, and Be impurity density were measured from charge-exchange recombination spectroscopy. Profiles of the carbon temperature T_{carbon} are shown in figure 2(*a*).

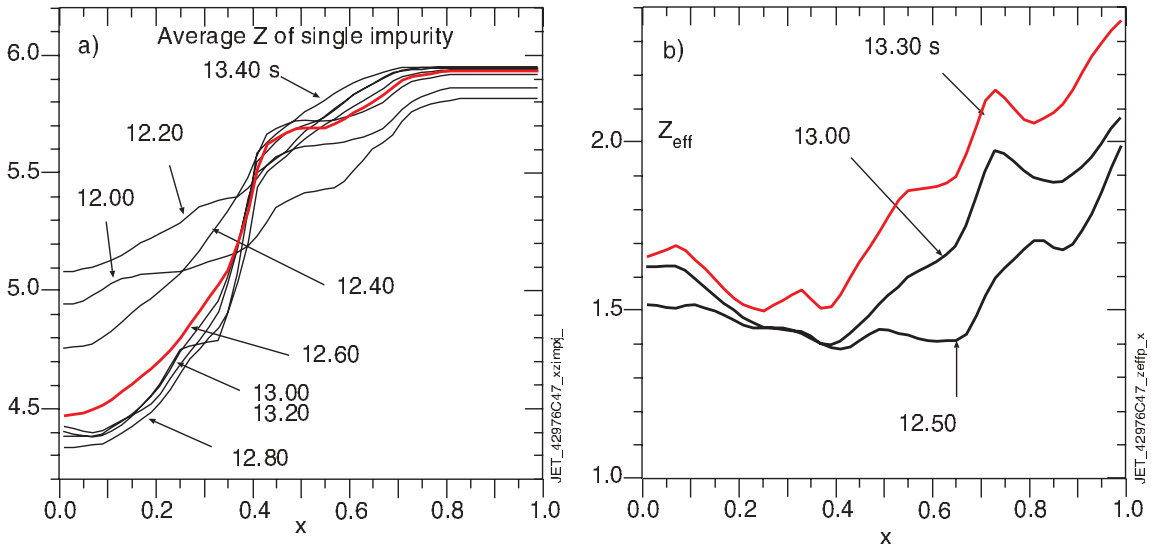

Figure 3. Profiles of the (*a*) impurity effective Z computed from measured n_{carbon} and n_{Be}; (*b*) Z_{eff} computed from Z and n_{carbon} and n_{Be}.

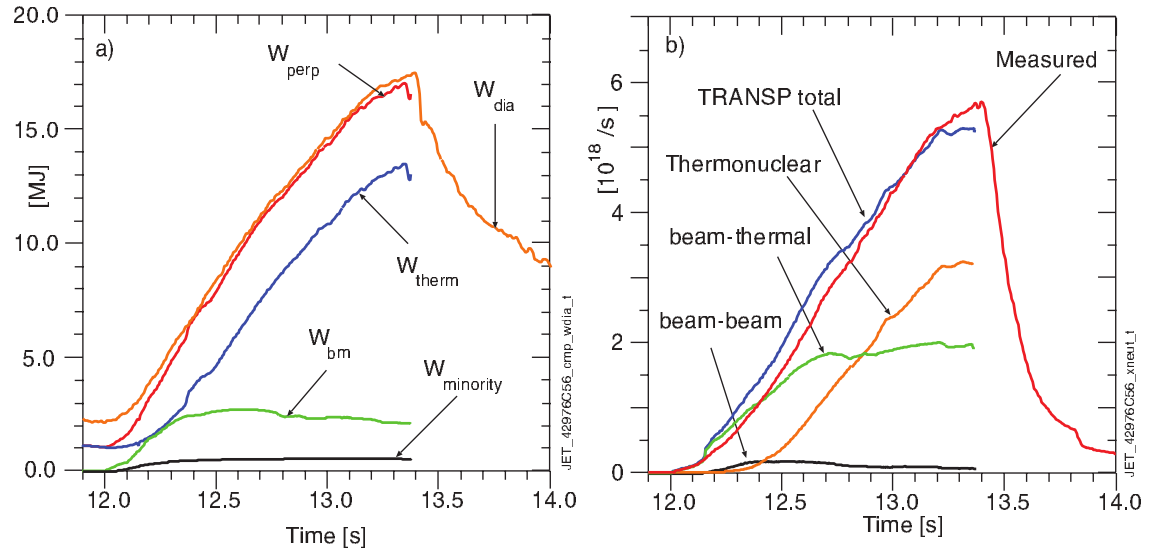

Figure 4. Time traces of (*a*) the measured diamagnetic and TRANSP-simulated perpendicular energies, and (*b*) measured and TRANSP-simulated neutron emission rate in JET.

The measured helium density was relatively small (and with large uncertainty) and is ignored here. The Be density is centrally peaked and the C density edge peaked, as shown in figure 2(*b*). The measurement errors for the concentrations of carbon $C_C \equiv n_C/n_e$ and beryllium $C_{Be} \equiv n_{Be}/n_e$ are $\pm 7\%$ and $\pm 25\%$ respectively.

The profile of the average charge Z density-weighted from C and Be

$$Z = (4n_{Be} + 6n_C)/(n_{Be} + n_C) \tag{2}$$

is shown in figure 3(*a*). This is hollow in the core which is consequential for the dilution of n_D and n_T and the neutron emission simulations.

Using charge neutrality, the profile of Z_{eff} is given in terms of the concentrations C_{Be} and C_C by

$$Z_{eff} = 1 + 4 \times 3 \times C_{Be} + 6 \times 5 \times C_C \tag{3}$$

The values increase from 4.7 to 5.5 at flat top, as shown in figure 3(*b*).

TRANSP computes an effective single species impurity profile n_x that can be used with Z to compute Z_{eff}:

$$Z_{eff} = 1 + Z \times (Z - 1) \times n_x/n_e \tag{4}$$

For many JET *DT* discharges and most TFTR discharges, at most one impurity (C) density profile is known. In some of the JET discharges carbon density profile and the ratio n_{Be}/n_C at one radius were measured. These measurements have been used in most of the TRANSP analysis runs with Z assumed to be flat in radius. With this, dilution effects can be approximated using the n_C shape for n_x.

4. Tests of the accuracy of the JET simulations

The TRANSP simulations are tested by comparing with measurements. A run (with the IC kick operator) is compared with the EFIT calculated diamagnetic energy in figure 4(*a*). Approximate agreement is achieved during the ramp-up phase, but TRANSP is low for the last 30ms before the time of the end of charge-exchange measurements. Uncertainty in the pedestal and boundary location contribute to uncertainty in the TRANSP simulation. The global neutron emission rate S_n is compared in figure 4(*b*). Approximate agreement is achieved during the ramp-up phase, and then TRANSP is 10% lower than the measurement. The under-prediction of the global neutron emission rate suggests that the core Z might not be as low as modeled. There are no ion temperature, impurity, or rotation profile data after 13.365 s so extrapolations after that time are not credible.

The IC direct power deposition computed by the TORIC module in TRANSP was mainly on the H-minority (58%), the thermal D (15%) and the fast D (15%) ions, and electrons (9%). The direct IC power deposited on the thermal and fast T ions was small (<1%). The IC resonance location for the T beam ions is on the inside and the kick operator deaccelerates them, or ejects them past the boundary. Even though the computed (pre-kick) deposited power is relatively small, the effects of the kicks can change the beam energy distributions significantly. The D beam energy tail is extended and the T beam tail energy is reduced. The net effect reduces S_n by 10% compared with the equivalent TRANSP run without the kick operator.

A stronger test of the simulated DT neutron emission is comparison with measured profiles of the emission. A neutron detecting camera system is used for measuring neutron emission rate along 19 sight lines, as shown in figure 5. TRANSP simulations of the neutron emission rates in the core and profiles near the peak are compared with fits to the data in figure 6. The peak is shifted outward slightly from the axis and the peak rates are under-predicted.

A TRANSP run was performed (without the IC kick operator) with the measured Be density scaled down by 25% (approximately one standard deviation) to test consequences if the measurement is too high by this amount. The under-predictions of the total and core neutron emission rates near the peak values are reduced, but not sufficiently to match the measurements.

Transp runs using the ripple model with nominal settings predict beam ion energy losses increasing to 8 MW, and lower the simulated S_n by 12% and $S_n(0)$ by 8%. Calibration of the ripple criterion could significantly change these predictions.

5. p_α and q_{DT} in JET

The baseline TRANSP analysis run (with IC kicks and without ripple loss) is used to study electron heating, losses, and flows. The net electron heating p_e is time and volume integrated as in [23]. Profiles of the results shortly before the disruption are shown in figure 7(*a*). The plots show multiple processes competing with $p_{\alpha e}$. The time and volume-integrated to $x = 0.3$ evolution is shown in figure 7(*b*). Several terms remain comparable to $p_{\alpha e}$. Figure 8 shows heating profiles at a time near

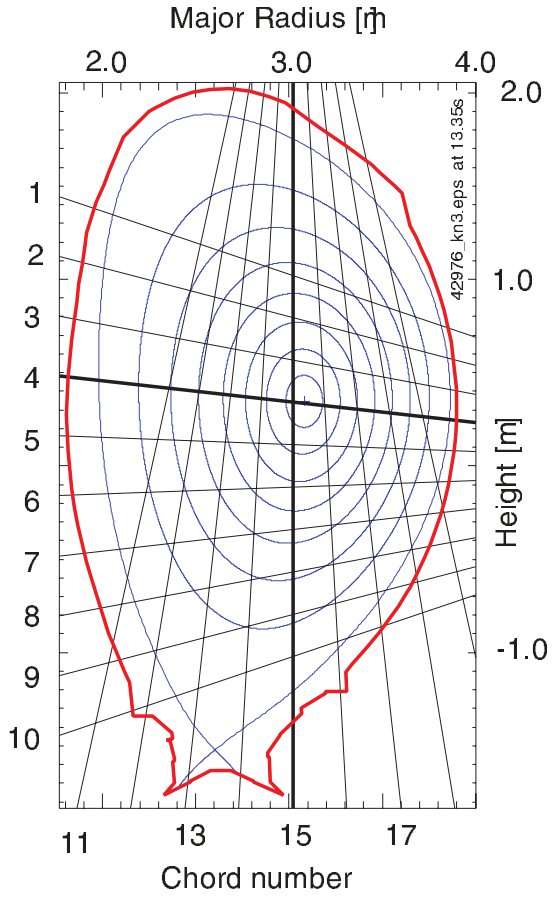

Figure 5. Schematic of the JET neutron collimator camera sight lines.

peak p_{DT}. In steady state, and neglecting fast alpha losses from the plasma, the rates of fast alpha production p_{DT} and alpha heating p_α should reach a constant ratio. The partition of fusion energy to neutrons and fast alpha ions is 80 : 20 so the alpha heating p_α would be $p_{DT}/5$. This is predicted to be low by a factor of two. This under-prediction is attributed to the short duration of the high p_{DT} phase compared with the alpha slowing down time. The slowing down time of the fast alpha particles in the core is 1.2 s.

A range of profiles of q_{DT} is included in figure 9(*a*) to indicate numerical noise such as Monte Carlo noise in the calculations. The profile has a peak value near 1.2 on axis. Since the core neutron emission rate is underestimated by 20%, the actual peak value is expected to be closer to 1.4. The global Q_{DT} calculated is 0.68 at 12.25 s. The ratio of the p_α and p_{ext} in the core is shown in figure 9(*b*).

The new TRANSP runs have higher numerical accuracy and more complete physics than the runs used in [20], but the results for the maximum core q_{DT} derived from the previous runs are comparable.

Some other JET discharges achieved q_{DT} and Q_{DT} comparable to the results here. Several of the Hot-ion H-mode discharges from the alpha heating experiment [22] (42 847 and 42 856) achieved $q_{DT} \simeq 1.2$ and Q_{DT} near 0.7 [23]. The H-mode is taken to be the baseline regime for ITER. The JET

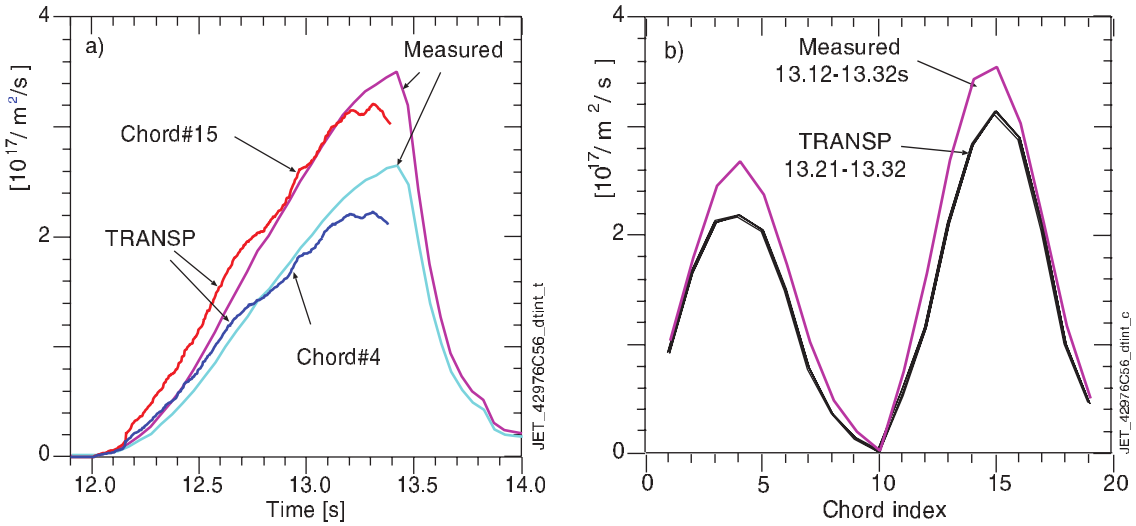

Figure 6. Comparison of fitted chordal measured and simulated neutron emission rates (*a*) time dependence; (*b*) profile just prior to the first giant ELM. The *x*-axis is the chord number. The measurement window for the charge exchange measurements ends at 13.364 s.

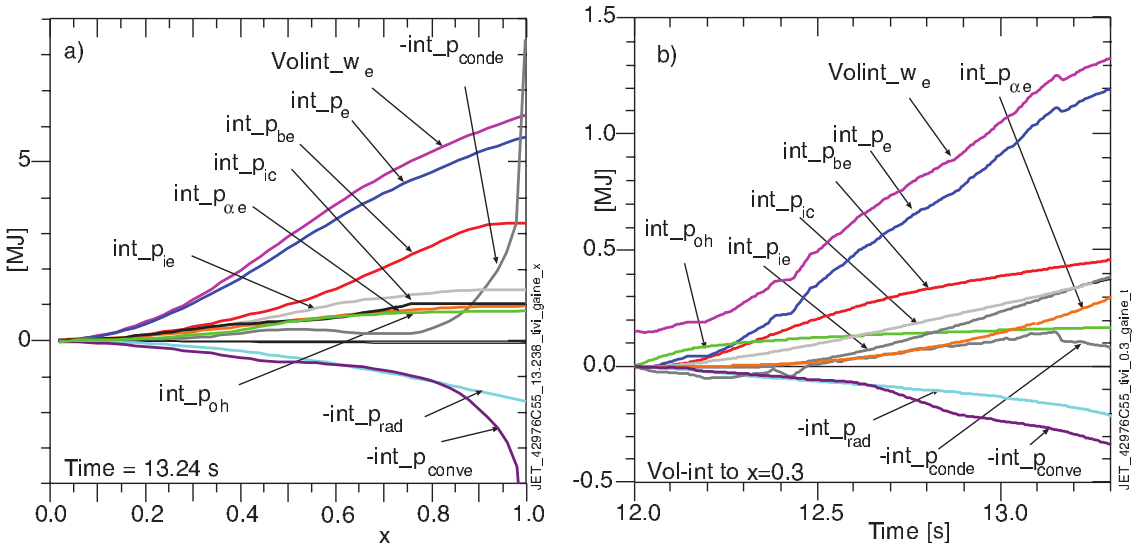

Figure 7. Time and volume-integrated electron heating and loss terms, and their sum p_e compared with the electron stored energy W_e: (*a*) profiles time integrated from 12.0 to 13.23 s; (*b*) time evolution volume-integrated to $x = 0.3$.

H-mode (42 982) with record P_{DT} (4.7 MW) is predicted to have core $q_{DT} = 0.7$ and $Q_{DT} = 0.28$ [25].

6. TFTR supershot with record P_{DT}

The TFTR plasma studied is the supershot [24] with highest P_{DT} [25] (80 539 in 1994). The auxiliary heating consisted of up to 25.3 MW of T-NB, 14.2 MW of D-NB between 3.3 and 4.2 s, and 0.5 MW Ohmic heating. This mix was chosen empirically to maximize the neutron emission rate S_n. Extensive diagnostic data exists for the time interval of the NB heating. The plasma current, major radius, and vacuum toroidal field were $I_p = 2.7$ MA, $R_0 = 2.52$ m, $B_0 = 5.5$ T. Some parameters are summarized in table 1.

This discharge was achieved with extensive wall conditioning. Two *Li* pellets were injected during the Ohmically-heated phases soon after 2.0 s (before the beam injection), and one at 4.5 s after the beam-heated phase. The purpose of the first two pellets was to coat the limiter to reduce the influx 'wall recycling' of hydrogenic ions from the limiter and walls. This resulted in achieving a low hydrogenic density in the edge, and allowing deep penetration of the NB neutrals and core ion heating which was necessary for the formation of supershots [26].

The purpose of the pellet after the NB phase was to prepare the limiter and walls for the next discharge. The amounts of *Li* entering the plasma can be calculated from the discontinuities of the measured electron density at the injection times [26]. The first two added 2.2×10^{20} and 3.1×10^{20} *Li* nuclei

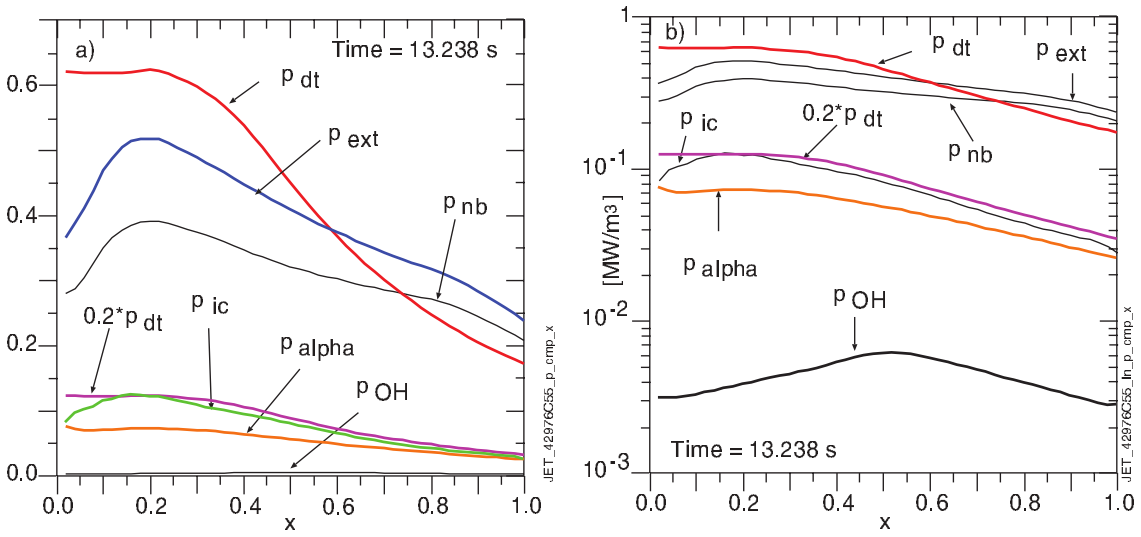

Figure 8. (*a*) Linear and (*b*) log plot of radial profiles of the volume-averaged heating powers just prior to the giant ELM.

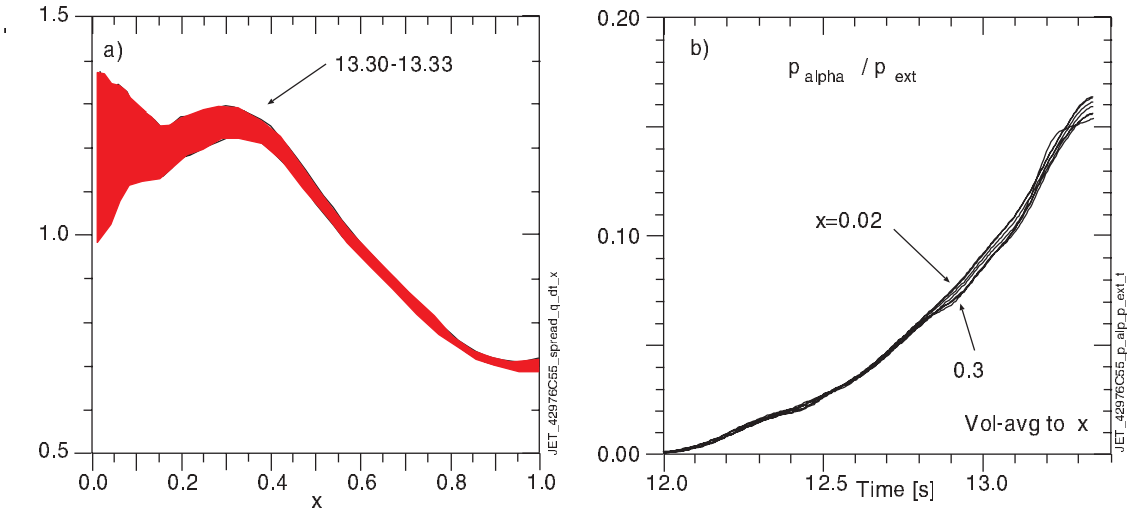

Figure 9. (*a*) Radial profiles of the q_{DT} (*a*) and ratio of p_α to $p_{\rm ext}$ within the CX measurement time window; (*b*) ratio of core alpha and external heating.

respectively assuming other impurities did not contribute to the time-discontinuity in n_e. TRANSP modeling of the *Li* evolution assuming the profile of the *Li* particle confinement time is the same as the other ions indicates that the *Li* concentration was relatively low (below 2×10^{17} m^{-3}) during the flattop.

The ratios of the *H*, *D*, and *T* emission in the edge were measured by a Fabry–Pérot interferometer [27]. The fraction of *H* was typically 10%. The *D* fraction generally dominated. The *T* fraction varied considerably in time, and correlated with the *T* beam injected in previous discharges.

The evolutions of the plasma species from two TRANSP runs are shown in figure 10. One run included *Li* and *H*. The total (volume-integrated) number from this run are shown in figure 10(*a*). The evolutions of the central densities from a run neglecting *Li* and are shown in figure 10(*b*).

The electron density and temperature data cover a long time window but the charge-exchange spectroscopy data exist only during the beam injection (between 3.3 and 4.05 s). Profiles of T_e measured by ECE versus electron-cyclotron frequency are shown in figure 11(*a*). Although the peak T_e was relatively high, some other TFTR discharges during later heavily lithium conditioned experiments had central T_e exceeding 15 keV. Thomson scattering measurements of T_e were available in earlier pre-DT phases of TFTR. Both measurements were in approximate agreement for T_e except for higher T_e ($\gtrsim$8 keV), as in the JET case where also ECE gave higher values.

The statistical uncertainty on the absolute T_e was $\pm$10%, independent of the value of T_e. The relative changes in T_e are known to an accuracy much greater than 1% since these are limited mainly by intrinsic photon noise.

The carbon ion temperature and toroidal rotation were measured by charge-exchange spectroscopy emission. Subtractions of background light were needed to calibrate the measurements. One method used data after the beam injection, but subtraction

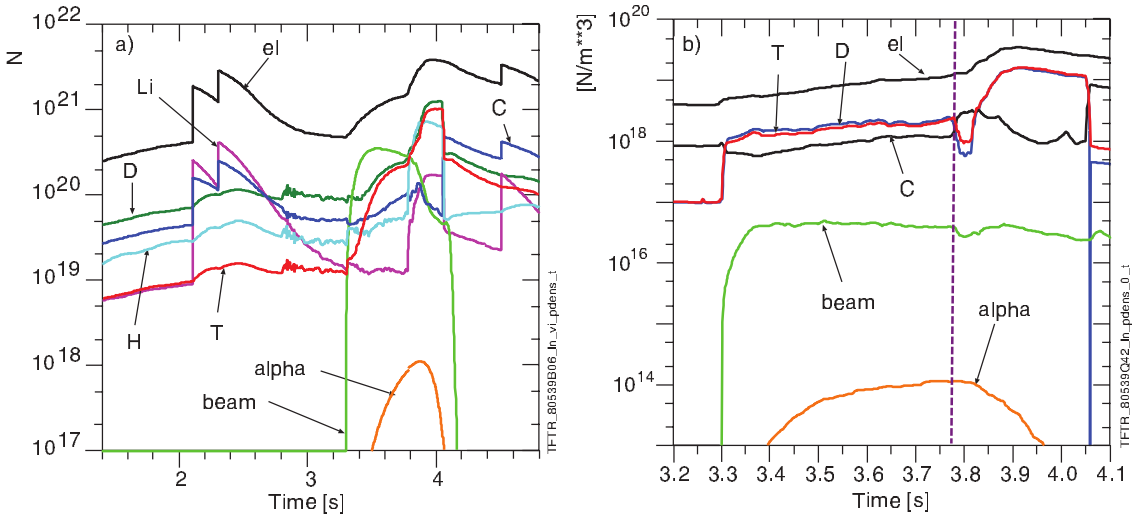

Figure 10. Time traces of (*a*) the total species numbers in TFTR from a TRANSP run including *H*, *D*, *T*, *Li*, and *C*; (*b*) species densities at the magnetic axis from a TRANSP run including *D*, *T*, and *C* with the effective charge *Z* varied in time. The time of the impurity bloom and minor disruption is indicated.

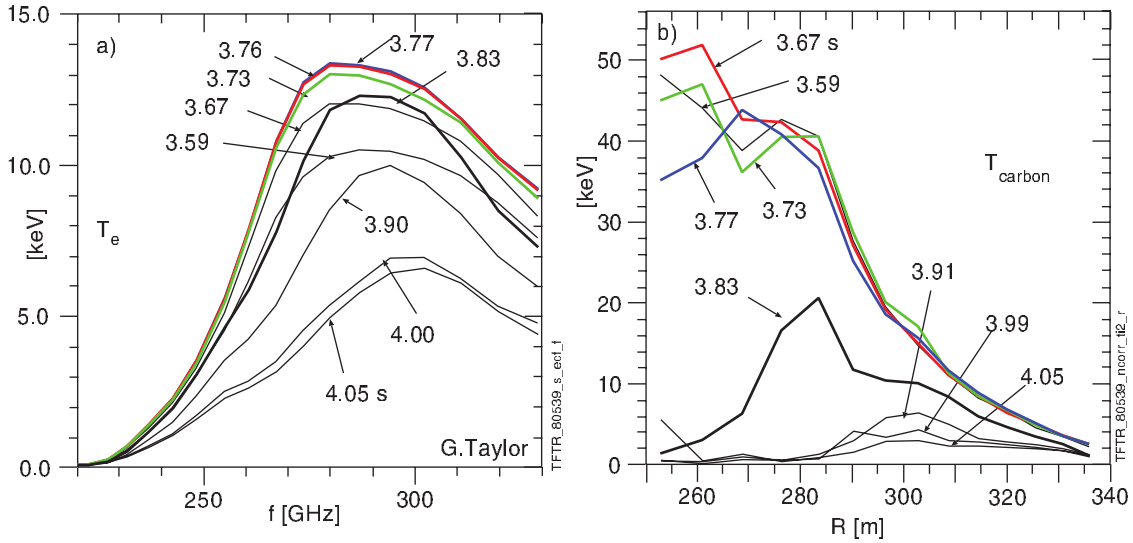

Figure 11. Profiles of (*a*) the electron-cyclotron measured electron temperature. The statistical uncertainty on the absolute T_e measured by ECE was $\pm 10\%$, independent of the value of T_e. (*b*) The charge-exchange spectroscopy measured carbon temperature.

for this discharge was complicated by large changes in n_e caused by the occurrence of the minor disruption discussed below. Several alternative methods were used to circumvent this. The most accurate used a radiating-shell model that estimated effects of the changing background by assuming all of the background light was emitted from a shell at the edge. The background light was reconstructed with a series of Gaussians whose amplitudes and widths and velocities are reconstructed from measurements.

An alternative method [28] used the background light from a similar but non-disrupted discharge. The results from this later method, considered to be much more reliable, are shown in figure 11(*b*). Core values are near the highest seen in supershots. The estimated error bars for the measurements are large, but fortunately the neutron emission rate simulations are insensitive to large variations of T_i with high values.

Profiles of n_e measured by interferometry are shown in figure 12(*a*). The plasma experienced a minor kink → ballooning disruption at 3.7847 s in the flat-top phase, followed by a rapid increase and broadening of n_e dubbed an 'impurity bloom'. Abrupt increases in CII emission were observed along several chords after 3.77 s.

This bloom caused the total number of electrons in the plasma to increase by a factor of 2.6 in 200 ms, with $\overline{n}_e$ increasing from 46% of n_{Gw} to nearly 100%, while broadening considerably. The peakedness defined by the ratio of the core to volume-averaged n_e drops from 2.75 to 1.3 in 75 ms.

There were radially in/out asymmetries after the disruption with peaking at small major radius near the toroidal limiter. The abrupt broadening and decay in time of n_e after this

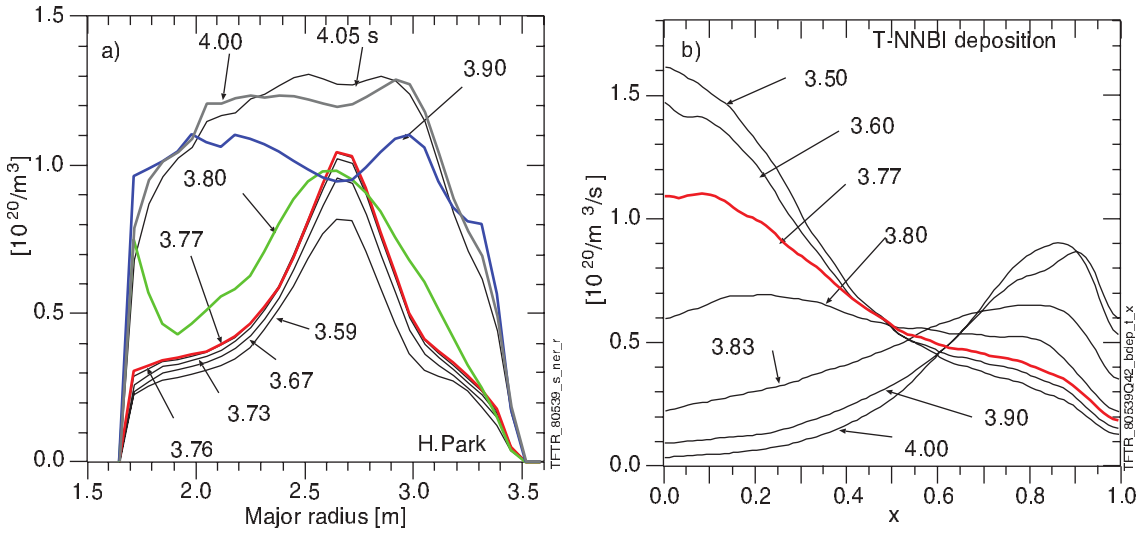

Figure 12. Profiles of (*a*) the interferometry measured electron density; (*b*) the tritium beam neutral ionization rate.

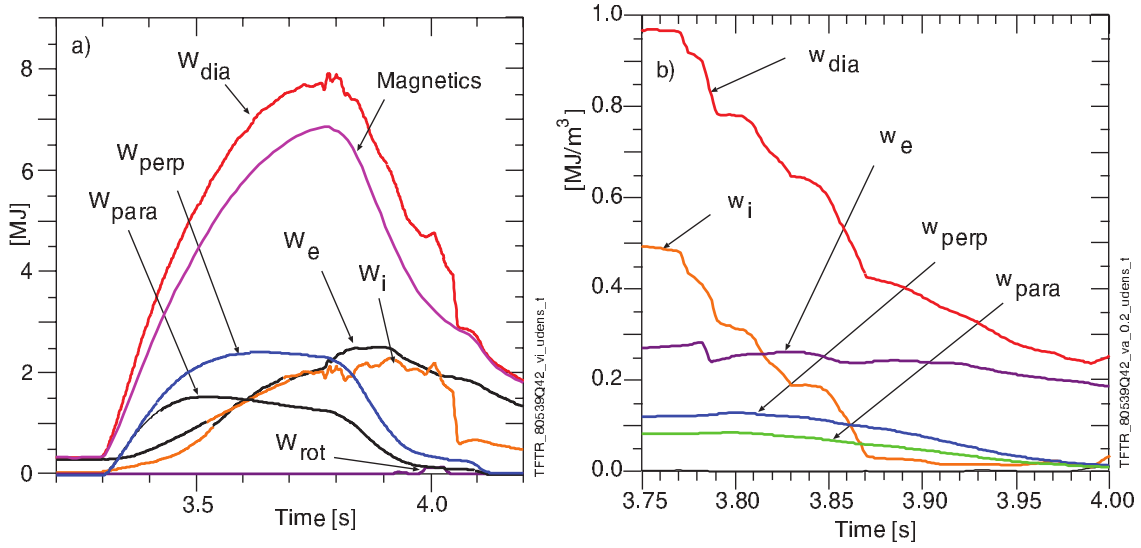

Figure 13. Time traces of the (*a*) magnetics measured stored energy and transp calculated stored energies in thermal electrons, ions, rotation, perpendicular and parallel fast (mainly beam) ions; (*b*) volume-averaged stored energies within the $x = 0.2$ flux surface normalized for comparison.

event was similar to the decay after pellet injections, with line-average $= 0.7 \times n_{Gw}$ by the time of the third *Li* pellet at 4.5 s.

The broadening of n_e caused the beam deposition peak to move from the axis to $x = 0.8$ by 3.8 s, as shown in figure 12(*b*). The peak beam density which peaked near $x = 0.35$ at 3.55 s moved to $x = 0.7$ by 3.95 s.

After the bloom, as the density increases dramatically the TRANSP computed hydrogenic ion temperature [29] dropped from near 43 to 3 keV between 3.75 and 3.8 s, and did not recover. The peak T_i became hollow after 3.8 s with peak near $x = 0.4$. The beam heating in the core reduced due to the drop in beam neutral ionization rate, as shown in figure 12(*b*).

The TRANSP computed stored energies are compared in figure 13(*a*). The TRANSP simulation is 15% higher than the measurement from magnetic signals. This discrepancy is addressed in the next section. The total W_{dia} is the sum of the fast ion perpendicular W_{perp} and parallel W_{para} energies and the thermal (assumed isotropic) ion $W_i = \int n_i \times T_i$ and electron $W_e = \int n_e \times T_e$ energies and a small contribution from the measured toroidal rotation. The fast ion perpendicular and parallel energies are dominated by the beam ions. The fast alpha peak contributions are 7–8% of the beam ion contributions. The beam ion contributions were generally relatively large in TFTR supershots early in the NB phase. The peak W_{perp} is larger than W_i and is nearly equal to the peak W_e contribution occurring later.

The total thermal ion stored energy W_i remains relatively constant throughout this drop as indicated in figure 13(*a*). The core thermal ion stored energy w_i drops rapidly as shown in figure 13(*b*).

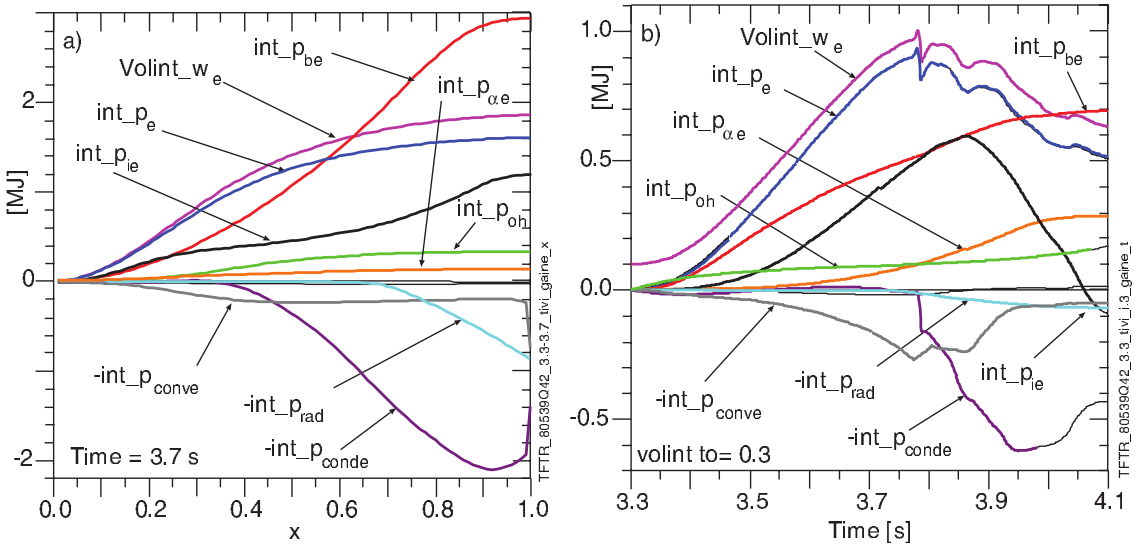

Figure 14. Time and volume-integrated electron heating and loss terms and their sum p_e compared with the electron stored energy W_e: (*a*) profiles time integrated from 3.3 to 3.7 s of the (*b*) time evolution volume-integrated to $x = 0.3$.

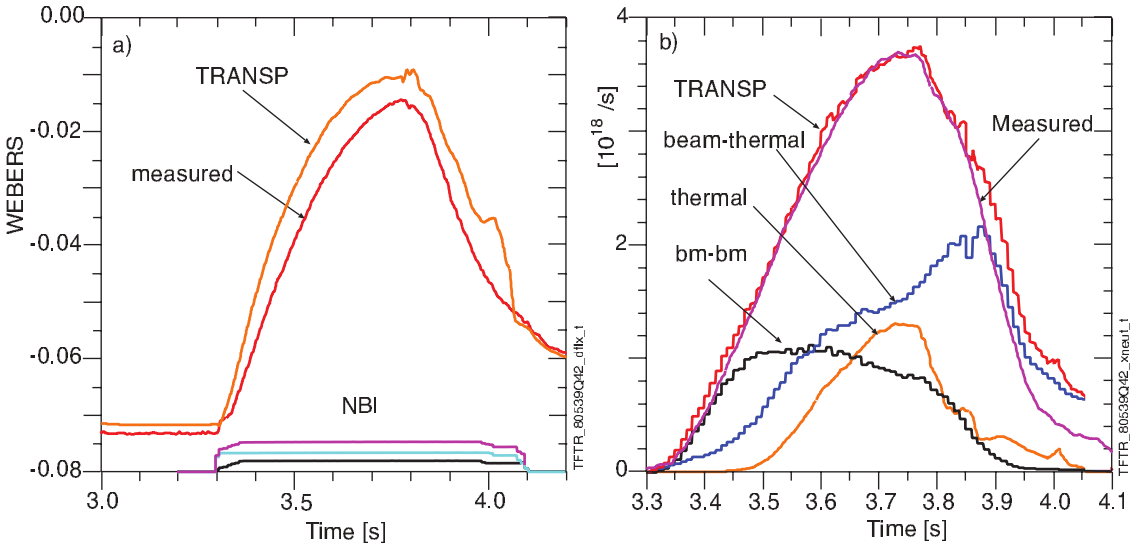

Figure 15. Time traces of (*a*) the TRANSP-simulated and measured diamagnetic flux, with a schematic of the NB heating D and T powers, and (*b*) neutron emission rates in TFTR. The measurements of T_i and n_x extend from 3.3 to 4.05 s.

The central electron temperature drops from a peak of 13.5 at 3.777 s to 11.3 keV at 3.778 s, then increased to 12.2 keV at 3.84 s. The volume-averaged and core electron energy densities shown in figure 13 are relatively constant. There is rapid flow of energy between ions and electrons since they are out of equilibrium. The flow direction is from thermal ions to electrons before the T_i collapse, and then reverses sign.

The volume-average flow in the core to $x = 0.2$ is shown in figure 14. The alpha and beam ion heating adds to the electron heating, but they are dominated by the equilibration flow except near 3.85 s. The computed peak alpha heating power density which was $\simeq$0.24 (MW m^{-3}) immediately after the disruption increased to 0.27 at 3.84 s. Thus rapid equilibration of energy between the electrons and ions complicates observation of alpha heating effects. Other energy sources such as beam heating also contribute to the energy balance.

Absolutely calibrated charge-exchange spectroscopy measurements of impurity densities were not available in TFTR. The relative profiles of the carbon density were normalized using a well-calibrated visible bremsstrahlung emission measurement along a chord. Since TFTR had a circular cross section with a large toroidal limiter, interpretation of this signal was relatively uncomplicated. The density profiles of other impurities were not measured so an effective charge Z is assumed for a single effective impurity n_x species with the shape of the normalized carbon density.

7. Tests of the accuracy of the TFTR simulation

The minor disruption challenged and added uncertainty to the measurements. The core q_{DT} appeared to have reached above unity after the event, but this is not conclusive due to uncertainties. An analysis is given below with the goal of indicating challenges and issues facing future measurements of alpha heating.

Tests of the accuracy of the simulated stored energies are shown in figures 13(*a*) and 15(*a*). Figure 15(*a*) compares the simulated and measured diamagnetic flux. TRANSP is high approximately 5 mWb, about 10%. The discrepancy of 5 mWb corresponds to almost 0.6 MJ in plasma stored energy. The over-prediction in the pre-NB phase could be caused by an over-estimate of T_i when it was not measured, but this contribution is small. The over-prediction during the NB phase could be attributed to various causes such as uncertainties in the measurements or in the TRANSP calculation of the fast ion perpendicular contributions.

Runs were performed varying input plasma profiles from their measured values. Variations of the measured n_e ±10% had very little effect on the diamagnetic flux due to compensating effects. Variation of T_e scaled down 10% reduced the discrepancy in the diamagnetic flux in the flat top phase by one half, while increasing the simulated S_n. Likewise variation of T_i scaled down 10% reduced the discrepancy in the diamagnetic flux in the flat top phase by 40% with little change in the simulated S_n.

The true value of the perpendicular fast ion energy density could be less due to ripple losses, to inaccuracies in the calculated pitch-angle scattering, in the beam ion deposition, or to anomalous fast ion diffusion.

Ripple losses of beam ions are expected to be relatively large at late times in this discharge since the high core density resulted in shifting the beam ion profiles toward larger radii where the ripple was larger. The stochastic ripple loss model [16] in TRANSP calculates the ripple loss of beam ions to increase to 3.8 MW by the time of the disruption, then to 5.8 MW at 3.9 s. The simulated number of total beam ions is reduced 15% and the diamagnetic flux by 1 mWb.

A TRANSP run was performed turning off the pitch angle scattering to assess effects of potential inaccuracy in the calculation of the anisotropy of the fast ion distributions. In this case the perpendicular and parallel fast ion energy densities depend only on the beam injection angles and the fast ion collisional slowing down. The resulting perpendicular fast ion energy density is reduced in the core by about 15% and the parallel fast ion energy density increased by the same amount. The resulting changes in the diamagnetic flux and S_n are several percent. Thus inaccuracies in the pitch-angle scattering, perhaps due to uncertainty of the impurities do not appear to resolve the discrepancy of the diamagnetic flux.

No evidence of fast anomalous ion diffusivity has been found in TFTR except in discharges with relatively low I_p or with highly reversed magnetic sear (enhanced reverse magnetic shear 'ERS'). Never-the-less TRANSP runs were performed assuming an ad hoc fast ion diffusivity D_{eff} with temporal but not spatial variation. Temporal variation of D_{eff} from 5 $m^2\ s^{-1}$ at the start of NB to below 0.1 $m^2\ s^{-1}$ from 3.4 to 3.85 s is sufficient to simulate agreement. TRANSP simulations of some discharges with intense Alfvén mode activity or highly reversed magnetic shear require comparable or larger values of D_{eff} for agreement. This value adversely impacts agreement with the neutron measurements discussed below.

Results from TRANSP analysis reported shortly after the experiment had a discrepancy of about 3 mWb, half of the nominal result reported here. One difference is those earlier runs assumed the ripple model, which is not considered to be accurate. To summarize, no plausible single perturbation of the TRANSP simulations was found to resolve the discrepancy of the over simulation of the diamagnetic flux (without worsening the agreement with neutron emission, discussed next). Fast ion anomalous diffusion alone does not appear plausible. Various double perturbations might resolve the discrepancy. Examples are ripple loss of beam ions and overestimation of T_e or T_i.

The global neutron emission rates S_n are compared in figure 15(*b*). TRANSP is close to the measured rate until 3.85 s. The beam-thermal and thermonuclear fusion reactions dominate the total around these times. The TRANSP run varying D_{eff} for agreement with the diamagnetic flux under-predicts the measured S_n by up to 15% in the flat top phase.

The simulated S_n depends moderately sensitively on Z up to the time of the disruption. Approximate agreement with S_n is achieved with Z rising steadily from 4.5 at the start of the NBI to 6 at 3.78 s, just after the abrupt increase in the CII emission. The large toroidal graphite limiter and other first walls were coated with *Li* so Z between 3 and 6 is consistent with a mix of *C* and *Li*. Other impurities such as hydrogen buried in the limiter could have been released also. Values of Z above 6 have too low n_x and thus too little dilution of n_D and n_T, overestimating the neutron emission rate.

After 3.78 s the simulated S_n depends sensitively on Z and the best fit for Z decreases precipitously to 3.8 within 20 ms. The decrease suggests that the observed increase in n_e could have been caused largely by *Li* and/or hydrogenic influx. Alternatively higher Z impurities could be entering but remaining outside the core region where most of the neutrons are emitted. During the next 20 ms the Z for best fit to S_n increases to 4.5 by 3.82 s. A good fit for later times was not found.

Alternative simulations assuming increased recycling of H after the bloom also achieve approximate agreement with the global neutron emission rate. The species number from such a run is shown in figure 10(*a*). The total rate of recycling hydrogenic species was held fixed, but the partition of H was increased at the disruption. The ratio of H to $H + D + T$ in the core increases from 5 to 8% at the disruption, then increases to 12–18%.

8. q_{DT} and p_α in TFTR

To accurately predict p_{DT} in the core, the core neutron emission rate needs to be accurately simulated. Since uncertainties in the plasma profiles after the disruption are relatively large, we focus on the simulation before that time. Figure 16 compares the TRANSP-simulated neutron emission rates viewed

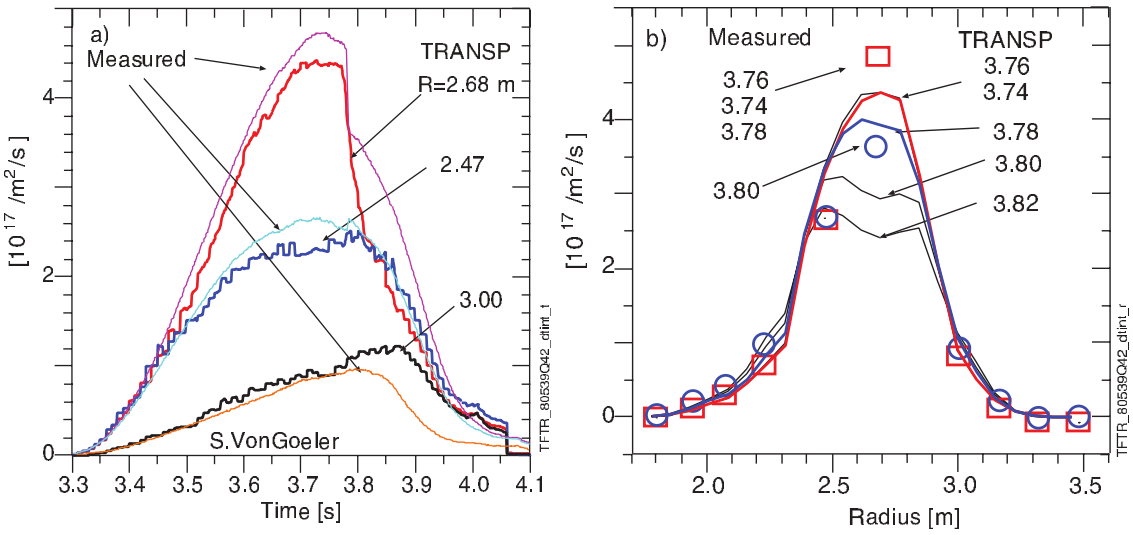

Figure 16. (*a*) Measured chordal neutron rates versus time; (*b*) TRANSP-simulated and measured chordal neutron rates at time of peak rate in TFTR.

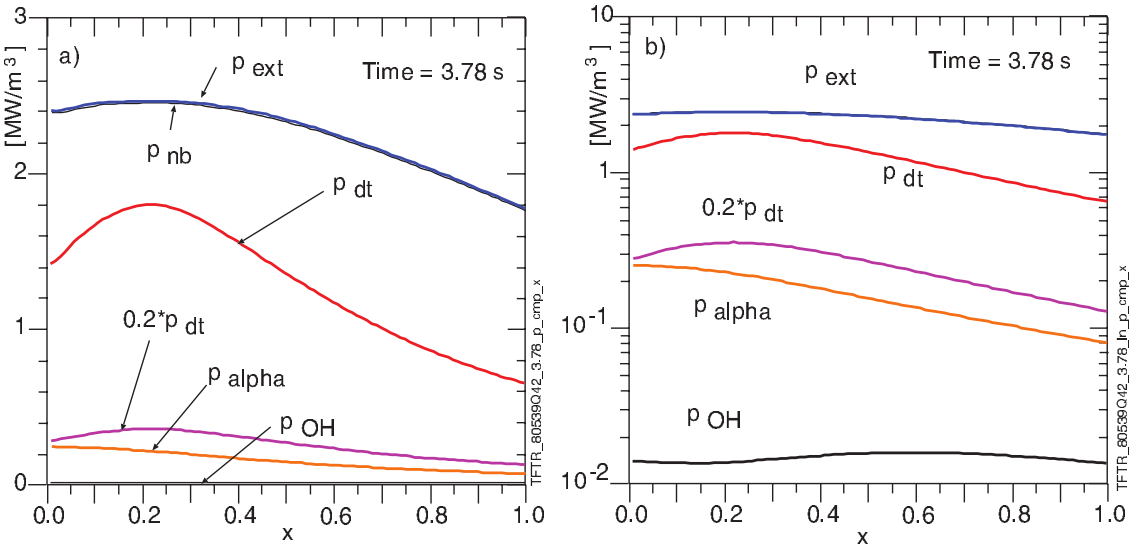

Figure 17. Plots of radial profiles of the volume-averaged heating powers (*a*) just prior to the minor disruption, and (*b*) semi-log plot. The *DT* power p_{DT} is computed from the *DT* neutron emission rate. In steady state the alpha heating rate is approximately 20% of p_{DT}.

by chords in an array of ten vertical neutron detectors [30]. The simulation is 8% below the peak rate measured by the chord nearest the magnetic axis ($R = 2.68$ m) until 3.78 s indicating that $p_{DT}(0)$ is under predicted by this amount. At the minor disruption, the measured rate in the core channel drops from the peak by 20% in 2 ms. Between 3.78 and 3.82 s the simulated core rate continues to decrease below the measured rate indicating that the core n_x is too high and/or Z is too low. Profiles of the external heating $p_{\rm ext}$ are insensitive to the hydrogenic density profiles, but q_{DT} is very sensitive, so the simulation underestimates q_{DT} also by 8%.

Profiles of the plasma heating before the bloom are shown in figure 17. The dips in $p_{\rm ext}$ and p_{DT} near $x = 0.1$ are due mainly by dilution of the fuel by the centrally peaked n_x. The semi-log plot shows that the alpha heating is slightly more peaked than the external heating.

The partition of p_{DT} to alphas and neutrons is close to 1 : 5 so in steady state the alpha heating of the thermal plasma p_α would be $p_{DT}/5$ unless alphas are lost (considered to be insignificant). The results in figure 17 show that the p_α is lower by a factor of two. This is mainly due to the relatively long slowing down time (about 0.6 s) compared with the NB heating duration at flat top. TRANSP calculates negligible alpha loss from the plasma.

A range of profiles of q_{DT} is indicated in figure 18(*a*) to account for numerical noise such as Monte Carlo noise in the calculations. The profile has a peak value near 0.9 before the bloom. An 8% increase which would match the central collimator chord would increase the core q_{DT} to near unity. The calculated global Q_{DT} peaks at 0.285 between 3.75 and 3.77 s.

The ratio of the alpha heating to external heating is a metric for the accuracy of separating and measuring the alpha

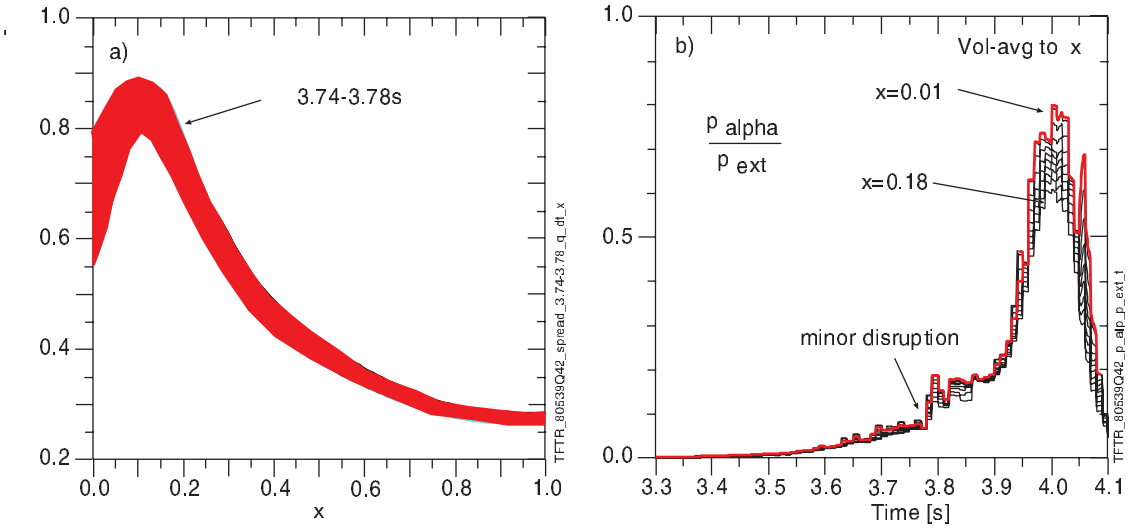

Figure 18. (*a*) Radial profile of q_{DT} near the time of the minor disruption; (*b*) ratio of core alpha and external heating.

heating. The central values for this ratio, shown in figure 18(*b*), increase to 0.9, assuming that the disruption did not expel the alphas. The peak ratio before the bloom is 0.075 (shown in table 1). This value increases during and after the bloom since the core beam penetration and heating decrease precipitously with the increased electron density after 3.78 s. The core alpha heating decreases less rapidly.

9. Predictions for an ITER baseline plasma

The plasma regimes of the TFTR and JET discharges (supershots and hot ion H-modes) discussed above are not considered to be practical or of interest for ITER. However, some of the issues challenging measurements of alpha heating might also challenge ITER.

There is an intense effort to simulate performance in ITER [31–38] Here we discuss results from an example of a self-consistent integrated prediction of an ITER baseline plasma using the TRANSP code. A new feature in TRANSP is used to predict impurity neoclassical flows with the NCLASS code [39].

The maximum NB voltage for the negative ion neutral beam injection (NNBI) is planned to be 1 MeV. An approximation to the 3D geometry of the sources, aiming angles, and beam ducts with a small footprint in the plasma and with below-axis aiming is assumed [32]. The IC is assumed to use ^{3}He as the minority ion species. The frequency is fixed at 52.5 MHz and the minority density ratio n_{He3}/n_e is assumed to be 0.02. Fundamental and harmonic heating of electrons and various ion species are computed. Codes for calculating IC in ITER have been benchmarked [40, 41]. The EC is assumed to be launched from three equatorial launchers and two upper launchers. The frequency is assumed to be 170 GHz, launched in O-mode. The divergence of the rays is assumed to be narrow (1.2°). Codes for calculating EC in ITER have been benchmarked [42]. The TORAY code [11, 12, 42] is used to model the ECH/ECCD. TORAY launched 20 rays from each antenna at each time step, and used 251 radial zones. Time dependencies of the plasma heating, total currents, and species are shown in figure 19.

One of the uncertainties for ITER baseline predictions involves sawteeth. With the assumed large total current (15 MA) relative to the driven currents, magnetic field diffusion is predicted to decrease the q profile in the core significantly below unity if sawteeth are not suppressed. Here we assume sawtooth breaks with period of 10 s. Kadomtsev helical flux mixing of the magnetic field, temperatures, and fast ion densities at these break times are assumed. The predicted current drive and mixing of the magnetic field results in the q profile remaining close to unity in the core, but with a q = unity surface near the mid-radius. Assumed Kadomtsev mixing of the fast beam ion and alpha densities predicts large transient perturbations at the crash times. Examples of such mixing are shown in [23].

Predictions of T_i profiles are needed to predict P_{DT}. Also density, T_i, and T_e profiles are needed to calculate heating. We use the GLF23 model [43, 44] which predicts T_i and T_e profiles in approximate agreement with current H-mode plasmas [45]. Temperature values at top of the pedestal T_{ped} are assumed for the boundary since the GLF23 model is not applicable in and beyond the pedestal. The pedestal temperatures are assumed to be around 5 keV. Time dependencies of the predicted core temperatures and their profiles at one time are shown in figure 20. The computed thermal energy and momentum diffusivities at one time between sawteeth are shown in figure 21(*a*).

The analysis of the JET and TFTR discharges described above indicated that dilution of the *DT* fuel in the core by impurities is significant. The planned ITER first wall will be dominantly tungsten and beryllium. Trace concentrations of *W* in the core can cause large amounts of radiation power loss without causing noticeable dilution; however the thermalized alphas 'ash' could have significant dilution effects if the transport is unfavorable. If the the fusion power were increased, for instance by increasing the pedestal temperatures, and if the transport remained fixed, the ash saturation level would increase, further

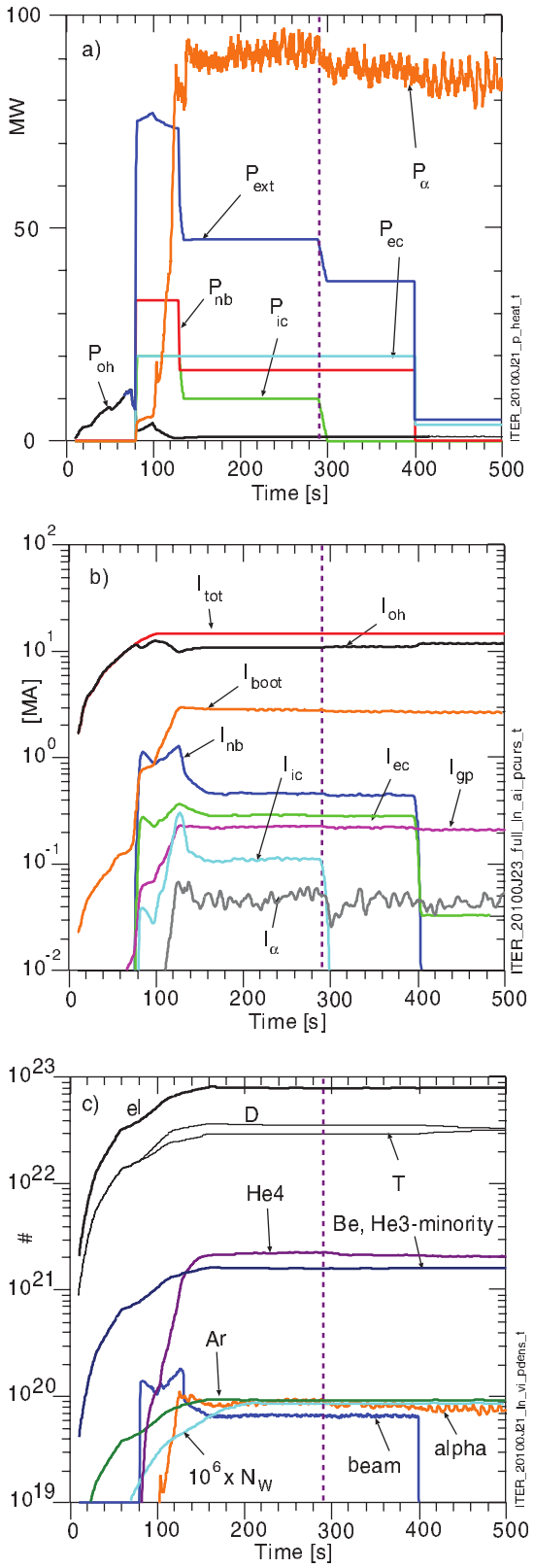

Figure 19. Predictions for a self-consistent ITER baseline plasma: time traces of (*a*) the heating powers and (*b*) plasma currents. The OH, EC, NB, and bootstrap current components of the total current are indicated; (*c*) volume-integrated species number.

diluting the *DT* density [34]. This would reduce the predicted Q_{DT} versus pedestal temperature dependence from the linear increase predicted with fixed n_{ash} [45]. Besides the ash, other impurities with moderate Z might accumulate in the core. For instance, there will be Be and perhaps puffing of noble gases such as argon or neon to enhance edge radiation.

For the ITER prediction we assume a n_e profile shape which is flat from the core to the pedestal, and which ramps up steadily until 160 s, reaching 0.86% of the Greenwald empirical limit. The impurities included are Be, Ar, *W*, and ash. Here the concentration of Be, Ar, and *W* were assumed to be fractions of n_e: 10^{-2}, 10^{-3}, and 10^{-6} respectively.

Transport of the ash is computed assuming that the ratio of ash returning into the plasma to exiting the plasma is 70%, and that the transport inside the plasma is described by a diffusivity of 1 $m^2\,s^{-1}$, and an inward pinch of 1 $m\,s^{-1}$. The computed ash profile saturates to one peaked near $x = 0.3$ with a minimum in the core of $0.02 \times n_e$ and maximum in the edge of $0.04 \times n_e$. Their total number is shown in figure 19(*c*). The ash confinement time is computed from these assumptions to be about 12 s compared with electron energy confinement time = 1.4 s and ion energy confinement time = 3.8 s. The contributions to Z_{eff} of the species are shown in figure 21(*b*). The assumed *W* concentration is small so its contribution to Z_{eff} is only 0.06. The assumed concentration of *W* increases the predicted total radiation by about 8% from 35 to 37.5 MW.

The predicted impurity neoclassical flows divided by densities are shown in figure 22. In the core the source of n_D is the NNBI fueling. The sink of n_D and n_T equal the fusion rate. Profiles of their neoclassical flows divided by their densities are shown at two times: 290 s during the crash when they peak flowing outward near the q = unity surface and 293 s between crashes when the flows are inward in the range of x shown. The flows are nearly equal, which would be advantageous for a reactor, facilitating maintenance of equal n_D and n_T in the core.

The neoclassical impurity flows during times between sawtooth crashes, and in the range of x shown are outward except for Be and the ash at large x. The densities n_{Be}, n_{Ar}, and n_W remain fixed at their ratios of n_e, except for n_{ash}, which is calculated,

Profiles of p_{DT} the heating are shown in figure 23(*a*). The peak in p_{ext} near $x = 0.15$ is due the peak in the below-axis NNBI heating. The peak near $x = 0.3$ is due to the EC heating. Unlike the results for the TFTR and JET cases, the alpha heating is close to $P_{DT}/5$. The slowing down time of the fast alpha particles in the core is 0.9 s. The q_{DT} profile is shown in figure 23(*b*) and compared with the JET and TFTR results. The dips in q_{DT} correspond to the peaks in p_{ext}. The q_{DT} profile peaks on axis with values up to ≃24. The global Q_{DT} is near 10.0. The ratio p_α/p_{ext} also peaked on axis up to ≃1–4.

10. Summary and discussion

TRANSP is used to calculate profiles of q_{DT} and alpha heating for the TFTR and JET plasmas with record values of global P_{DT}, and to predict profiles of q_{DT} and alpha heating for ITER. Accurate TRANSP modeling of heating powers requires

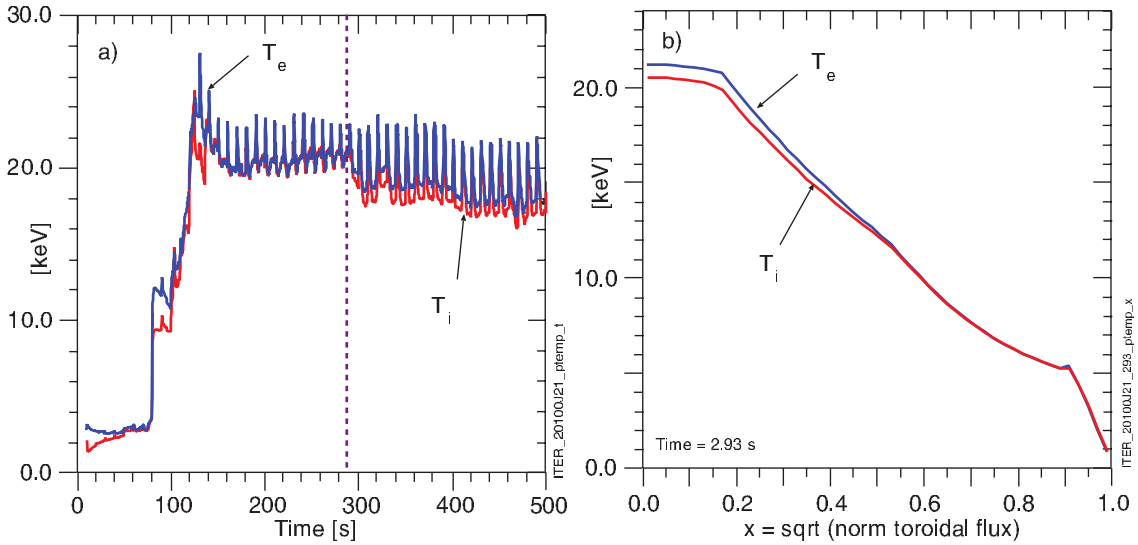

Figure 20. (*a*) Evolution of the GLF23-predicted core T_e and T_i showing effects of sawteeth crashes; (*b*) profiles at a time in the $P_{ext} = 48$ MW phase. $Q_{DT} = 9.8$ in this phase, then 11.8 after P_{ext} is decreased to 38 MW.

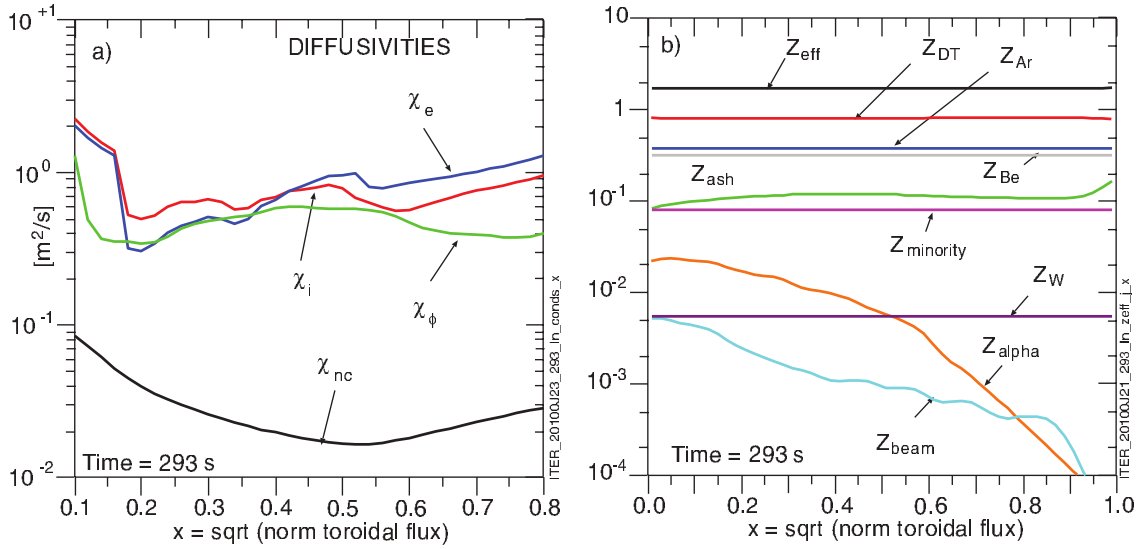

Figure 21. (*a*) Thermal energy and momentum diffusivities at times between sawtooth crashes (293 s); (*b*) profiles of the species contributions to Z_{eff} at 293 s.

accurate modeling of plasma profiles. To validate the modeling the stored energies and neutron emission rates of the TFTR and JET plasmas are compared with measurements. These rates are centrally peaked so accurate profiles in the core are especially crucial. Dilution of the n_D and n_T fuel by impurities is especially difficult to assess. One impurity density (carbon) in TFTR and three (carbon, beryllium, and helium) in JET were measured. The experimental uncertainties of the beryllium and helium measurements were large.

Other impurities could be playing significant roles. For the TFTR modeling the effective charge Z for the effective impurity with the density of the carbon was varied to achieve an approximate match of the global neutron emission rate. The value for the best fit increased from 4.5 at the start of the NB to 6 at the start of the minor disruption, suggesting that *Li* from the pellet limiter conditioning played a diminishing role near the flat top and time of the disruption. For the JET modeling runs using both the carbon and beryllium densities the values of of their average profile Z increased from the start of NB to 5.8 at the flat top and end of the data. The profile was lowest on axis and $\simeq$4.3 in the flat top. The simulations of the central neutron emission rate are low at the time of peak emission rate indicating that the modeled emission rate is insufficiently peaked.

The core q_{DT} computed by TRANSP is transiently near 1.3 for JET and 0.8 for TFTR. The simulated core *DT* neutron emission rate is low for TFTR (figure 16) and JET, figure 6(*b*) and thus the actual core q_{DT} are expected to be larger. Profiles of q_{DT} for the three plasmas are compared in figure 23.

Ratios of the core alpha and external heating are shown in figures 9(*b*) and 18(*b*). Qualitative evidence of alpha heating in

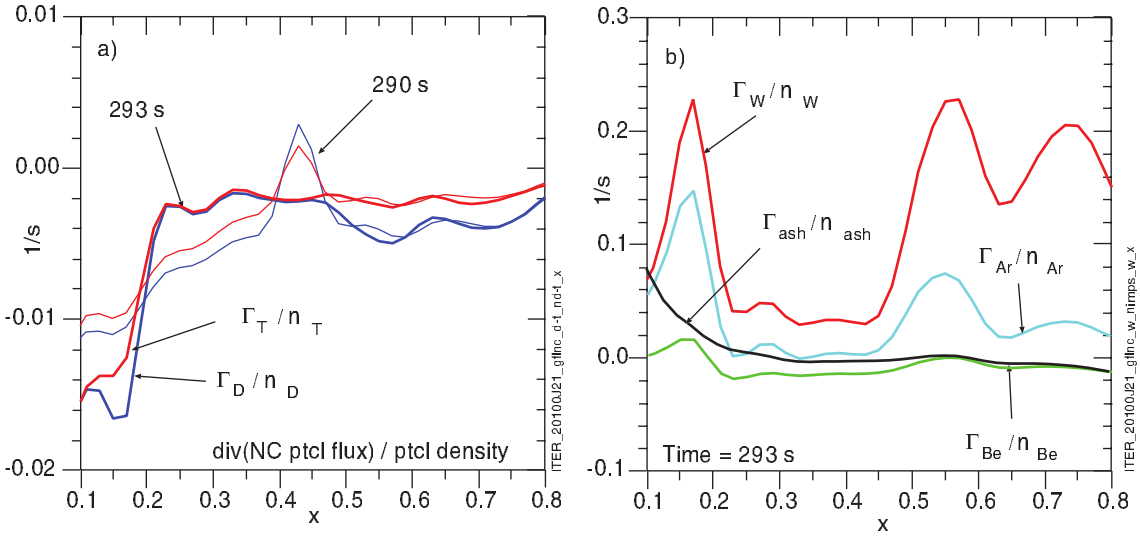

Figure 22. NCLASS neoclassical predictions of species flows divided by their densities of (*a*) thermal *D* and *T* at times between sawtooth crashes (293 s) and during a sawtooth crash (290 s); (*b*) impurity species between between sawtooth crashes (293 s) an ITER baseline plasma.

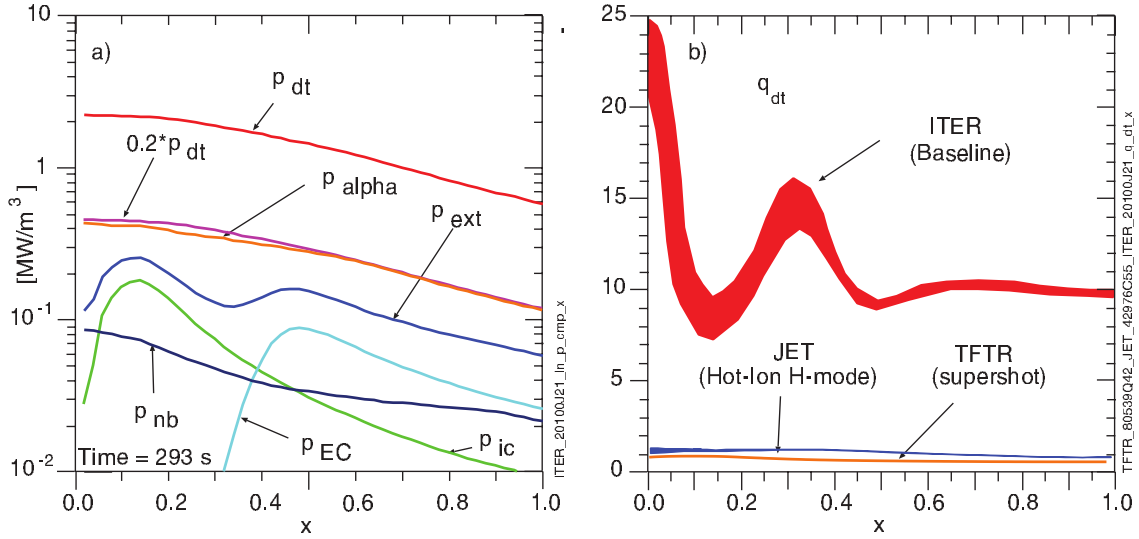

Figure 23. Radial profiles of the (*a*) volume-averaged heating powers and (*b*) q_{DT} in an ITER baseline predicted using GLF23 during the $P_{ext} = 48$ MW phase. The TFTR and JET q_{DT} profiles are included for comparison.

TFTR is seen in the resilience of T_e to collapse as T_i decreases precipitously after the minor disruption as shown in figure 11, and in the core w_e compared with w_i shown in figure 13.

These simulations suggest ways to more accurately quantify alpha heating in future experiments. The results in figures 17 and 8 show that p_α was below $0.2 \times p_{DT}$ due to the transient nature of the discharges. For the TFTR supershot the deficit was more than a factor of two. Shots with flattop phases lasting at least as long as the alpha slowing down times are desirable. Likewise sawteeth are expected to mix alphas and thus spread out the alpha heating profile, and thus sawteeth are undesirable. Peaked density discharges are also advantageous for peaking the alpha heating profile. Having *DD* and *TT* analogues of the *DT* discharges are also very desirable.

There are many uncertainties and new physics needed for making realistic predictions about burning plasmas. Among the poorly understood phenomena effecting uncertainty of the plasma parameters are the isotopic effects on the transport of particles, angular momenta, and energies. Proposed experiments in JET and ITER should result in important new insights and physics.

Acknowledgments

This work has been carried out within the framework of the EUROfusion Consortium, and has received funding from the Euratom research and training programme 2014–2018 under grant agreement No 633053. The views and

opinions expressed herein do not necessarily reflect those of the European Commission. This work was also supported in part by the US DoE contract No. DE-ACO2-76-CHO3073. The authors wish to thank D Meade for motivating this work, and M Bell, R Bell, E Fredrickson, G Taylor, M von Hellermann, and S Zweben for comments.

References

[1] Hurricane O.A. *et al* 2014 *Nature* **506** 343
[2] Goldston R.J. *et al* 1981 *J. Comput. Phys.* **164** 421
[3] Budny R.V. 1994 *Nucl. Fusion* **34** 1247–62
[4] Campbell D.J. 2001 *Plasma Phys.* **8** 2041
[5] Summers H.P. The ADAS User Manual v2.6 www.adas.ac.uk/manual.php
[6] Pankin A. *et al* 1981 *Comput. Phys. Commun.* **43** 61
[7] Bosch S. and Hale J. 1992 *Nucl. Fusion* **32** 611
[8] Brambilla M. 2002 *Plasma Phys. Control. Fusion* **44** 2423
[9] Budny R.V. *et al* 2016 ICRF acceleration of fast ions in TRANSP in preparation
[10] Hammett G.W. 1986 Fast ion studies of ion cyclotron heating in the PLT tokamak *PhD Dissertation* University Microfilms International No. GAX86-12694 (Princeton)
[11] Batchelor D.B. and Goldfinger R.C. 1980 *Nucl. Fusion* **20** 403
[12] Kritz A.H., Hsuan H., Goldfinger R.C. and Batchelor D.B. 1982 *Conf. Proc. 3rd Int. Symp. on Heating in Toroidal Plasmas ECE* (*Brussels, Belgium, 1982*) vol 2 p 707
[13] Shanny R. *et al* 1967 *Phys. Fluids* **10** 1281
[14] Budny R.V. and the TFTR group 1990 *J. Nucl. Mater.* **176–7** 427
[15] Voitsekhovitch I. *et al* 2014 *Nucl. Fusion* **54** 093006
[16] Goldston R., White R. and Booze A. 1992 *Phys. Rev. Lett* **47** 647
[17] Redi M.H. *et al* 1995 *Nucl. Fusion* **35** 1509–16
[18] Ruskov E. *et al* 1999 *Phys. Rev. Lett* **82** 924
[19] Baranov Yu.F. *et al* 2009 *Plasma Phys. Control. Fusion* **51** 044004
[20] Keilhacker M. *et al* 1999 *Nucl. Fusion* **39** 209
[21] De la Luna E. *et al* 2003 *Rev. Sci. Instrum.* **74** 1414
[22] Thomas P.R. *et al* 1998 *Phys. Rev. Lett.* **80** 5548
[23] Budny R.V. 2016 *Nucl. Fusion* **56** 036013
[24] Strachan J.D. *et al* 1987 *Phys. Rev. Lett.* **58** 1004
[25] Budny R.V. *et al* 2000 *Phys. Plasmas* **7** 5038
[26] Budny R.V. 2011 *Phys. Plasmas* **18** 092506
[27] Skinner C.H. *et al* 1995 *Nucl. Fusion* **35** 143
[28] Bell R.E., Synakowski E.J. and Bush C.E. 1994 *Program of the 1994 Annual Meeting of the Division of Plasma Physics* (*Minneapolis, Minnesota, 7–11 November 1994*) (*Bulletin of the American Physical Society* vol 39) p 6R11
[29] Budny R.V. *et al* 1992 *Nucl. Fusion* **32** 429
[30] Roquemore A.L., Bitter M., Johnson L.C. and von Goeler S. 1996 *Rev. Sci. Instrum.* **67** 544
[31] Kessel C.E. *et al* 2007 *Nucl. Fusion* **47** 1274
[32] Budny R.V., Andre R., Bateman G., Halpern F., Kessel C., Kritz A. and McCune D. 2008 *Nucl. Fusion* **48** 075005
[33] Halpern F.D. *et al* 2008 *Phys. Plasmas* **15** 062505
[34] Budny R.V. 2009 *Nucl. Fusion* **49** 085008
[35] Murakami M. *et al* 2011 *Nucl. Fusion* **51** 103006
[36] Kritz A.H. *et al* 2011 *Nucl. Fusion* **51** 123009
[37] Budny R.V. 2012 *Nucl. Fusion* **52** 013001
[38] Budny R.V., Yuan X., Jardin S., Hammett G., Grierson B.A., Staebler G.M. and Kinsey J.E. 2013 *EPS meeting Espoo* (*Finland, 2013*)
[39] Houlberg W.A., Shang K.C., Hirshman S.P. and Zarnstorff M.C. 1997 *Phys. Plasmas* **4** 3230
[40] Jaeger E.F. *et al* 2008 *Phys. Plasmas* **15** 072513
[41] Budny R.V. *et al* 2012 *Nucl. Fusion* **52** 023023
[42] Prater R. *et al* 2008 *Nucl. Fusion* **48** 035006
[43] Waltz R.E. *et al* 1997 *Phys. Plasmas* **4** 2482
[44] Kinsey J.E., Staebler G.M. and Waltz R.E. 2003 *Fusion Sci. Technol.* **44** 763
[45] Kinsey J.E., Staebler G.M. and Waltz R. E. 2008 *Phys. Plasmas* **15** 055908
[46] Romanelli F. 2015 *Nucl. Fusion* **55** 104001